



Overcoming the trade-off relationship between mechanical and adhesive properties of acrylic pressure sensitive adhesive thin-film by reinforcing polydopamine-coated silica nanoparticles

Seonghyun Kim^a, Seung Hui Lee^a, Subi Choi^a, Suk-kyun Ahn^{a,b}, Gi-Deog Jang^c,
Jong S. Park^{a,d,*}, Dong Gi Seong^{a,b,**}

^a School of Chemical Engineering, Pusan National University, Busan, 46241, Republic of Korea

^b Department of Polymer Science and Engineering, Pusan National University, Busan, 46241, Republic of Korea

^c R&D Center, YONWOO Corporation, Gyeonggi-do, 15602, Republic of Korea

^d Department of Organic Material Science and Engineering, Pusan National University, Busan, 46241, Republic of Korea

ARTICLE INFO

Keywords:

Adhesive film

Nanocomposite

Mechanical properties

ABSTRACT

PSA-silica nanocomposite thin-films with a thickness of 150 μm were newly fabricated through the optimized process to overcome the typical trade-off relationship where the enhancement of mechanical properties diminishes the strength of adhesive properties. As a consequence of reinforcement with polydopamine-embedded silica nanoparticles, the resulting nanocomposite films showed an 180% increase in tensile strength without a significant loss in peel strength. Viscoelastic behavior of the nanocomposite film was investigated to predict the final physical properties. Lap shear and probe tack tests were successfully performed to verify the reinforcing mechanism overcoming the trade-off relationship.

1. Introduction

Flexible, functional materials are of great interest in state-of-the-art electronic devices, such as foldable smartphones and rollable televisions, which require all constituting components to have a certain extent of flexibility. Flexible adhesives play a significant role in the assembly of these components [1,2]. Pressure-sensitive adhesives (PSAs) are non-reactive viscoelastic materials that form an adhesive bond between two materials by applying a slight pressure for a short time. PSAs are widely used in typical day-to-day applications, such as daily necessities, including tape, sticky notes, and food package labels, as well as structural materials for automobiles, construction, and medical applications. Therefore, due to its wide variety of usages, choosing the proper adhesive according to its physical properties is necessary for successful application to specific parts [3–7]. Moreover, thin-film type PSAs are required to satisfy form factors especially in slim-designed mobile applications.

Depending on their main functional group, several types of PSAs are present. Some commonly used PSAs are based on epoxy-, urethane-, acryl-, and silicone polymers. Among these, the acryl-based PSA has

many beneficial properties which include excellent transparency and environmental resistance to destructive factors, such as UV irradiation and chemical exposure. In addition, the versatility of the acryl monomer provides many options for modifying its physical properties and imparting various functionalities. However, unavoidable trade-off occurs between the mechanical and adhesive properties of PSAs, which are of great importance for industrial applications. That is, the adhesive force generally decreases when the formulation of a PSA mixture is changed to increase its mechanical properties, and vice versa [8,9].

Silica nanoparticles comprise Si–O–Si bonds and are strong inorganic materials with high mechanical and thermal properties that can be relatively easily synthesized in various shapes and sizes. These nanoparticles are frequently used as reinforcement for polymer resins and rubbers. Their common purpose is to improve the mechanical and thermal properties of the polymer matrix, but they can also be employed for other beneficial properties, such as controlling the viscosity of polymer melts and adding adhesion for biological tissues and soft polymeric hydrogels. Furthermore, these reinforcement effects can be further enhanced by functionalizing the surface of the nanoparticles [10–16].

* Corresponding author. School of Chemical Engineering, Pusan National University, Busan, 46241, Republic of Korea.

** Corresponding author. School of Chemical Engineering, Pusan National University, Busan 46241, Republic of Korea.

E-mail addresses: jongpark@pusan.ac.kr (J.S. Park), dgseong@pusan.ac.kr (D.G. Seong).

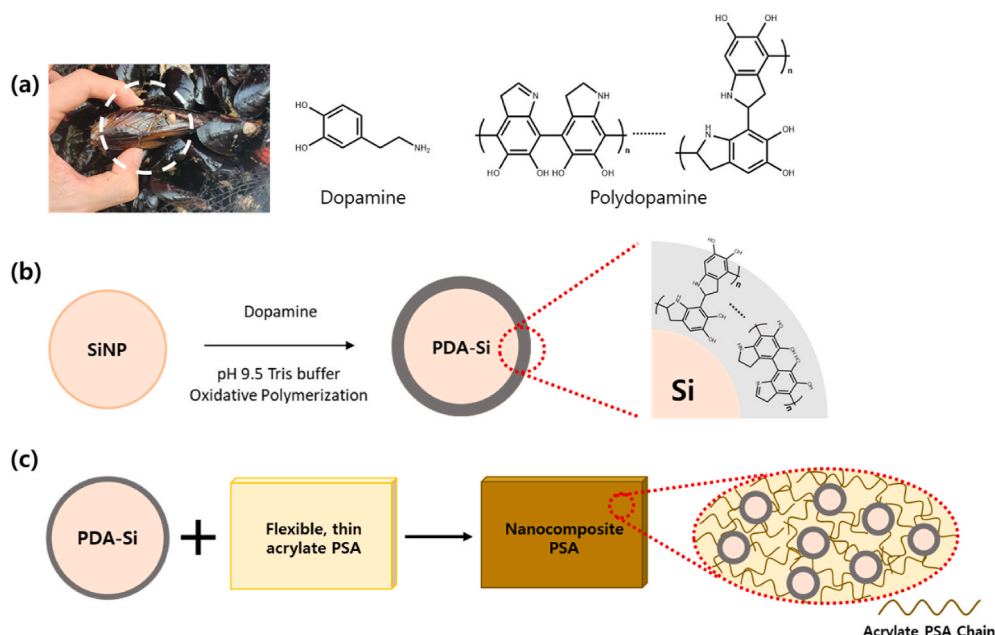


Fig. 1. (a) Photograph of a mussel and the chemical structure of dopamine and polydopamine. (b) Schematic diagram of polydopamine coating process on silica nanoparticle and anticipated chemical structure of PDA-coated silica nanoparticle. (c) Schematic process of the fabrication of nanocomposite PSA reinforced with polydopamine coated silica nanoparticles.

Table 1

Chemical composition and structure of acrylic PSA mixture.

Chemical	Chemical Structure	Weight Percent (wt%)
2-Ethyl hexyl acrylate		77.6
Acrylic acid		14.6
Tetrahydrofurfuryl acrylate		1.5
Terpene oil		5.9
1,6-Hexandiol diacrylate		0.2
Irgacure® 819		0.2

As shown in Fig. 1 (a), mussel-inspired polydopamine is well-known as a highly adhesive material regardless of its surface type of attaching substrate. It can be easily synthesized in base buffer solution by oxidative self-polymerization of dopamine, comprising catechol and amine [17]. Numerous studies have focused on its exceptional adhesiveness and ease of synthesis, and various kinds of application have been reported [18–22]. For example, Ang et al. [20] reported developing a high-performance nano-filtration membrane with polydopamine-coated silica nanoparticles using polydopamine's strong adhesive properties. And Lee et al. [21] coated polydopamine on carbon fiber surfaces to enhance the physical properties of carbon fiber reinforced plastics. Furthermore, Zou et al. [22] coated the polydopamine on the wood

surface with arginine to develop novel solar vapor generation system.

Understanding the mechanism of adhesion and failure is another crucial aspect for analyzing and improving the properties of PSAs. Monitoring the viscoelastic behavior of polymeric materials affords us a better understanding of their various physical properties. If we compare the viscoelastic parameters, including the storage modulus (E' or G'), loss modulus (E'' or G''), and $\tan \delta$ (Tan δ), we can predict the physical properties. In addition, the trend of peel strength can be determined when we investigate the loss moduli at specific frequencies. For example, Lee et al. [23] determined the relative peel strength of 2-ethyl hexyl acrylate (2-EHA) based adhesive films by comparing loss modulus (G'') at 100 Hz. Moreover, we can anticipate which PSA film has a higher cohesive strength by observing the storage modulus [24]. A rheometer has been frequently used to scan the viscoelasticity of PSA films. Dynamic mechanical analysis (DMA) can also be used to provide the viscoelastic parameters of polymeric materials [25–28].

The main objective of this study is to propose a fabrication method for overcoming the typical trade-off relationship by concurrently enhancing the mechanical and adhesive properties of PSA film (~150 μm of average thickness) with the aid of polydopamine functionalized silica nanoparticles. Schematic illustrations demonstrating this approach are shown in Fig. 1(b) and (c). We observed the viscoelastic behaviors of PSA films to predict their mechanical and adhesive properties and investigated them by comparing with the related experimental results including tensile, lap shear strength, probe tack, and 180° peel strength, from which we could understand the reinforcing mechanism in the nanocomposite PSA films and demonstrate that observation of the viscoelastic behavior could be utilized to predict their physical properties.

2. Experimental

2.1. Materials

UV-cure type acrylic PSA mixtures based on 2-ethyl hexyl acrylate (2-EHA) and acrylic acid (AA) monomers were supplied by YONWOO Corp. (South Korea), and the chemical composition of the mixtures are listed in Table 1. Silicon dioxide nanoparticles with an average size of

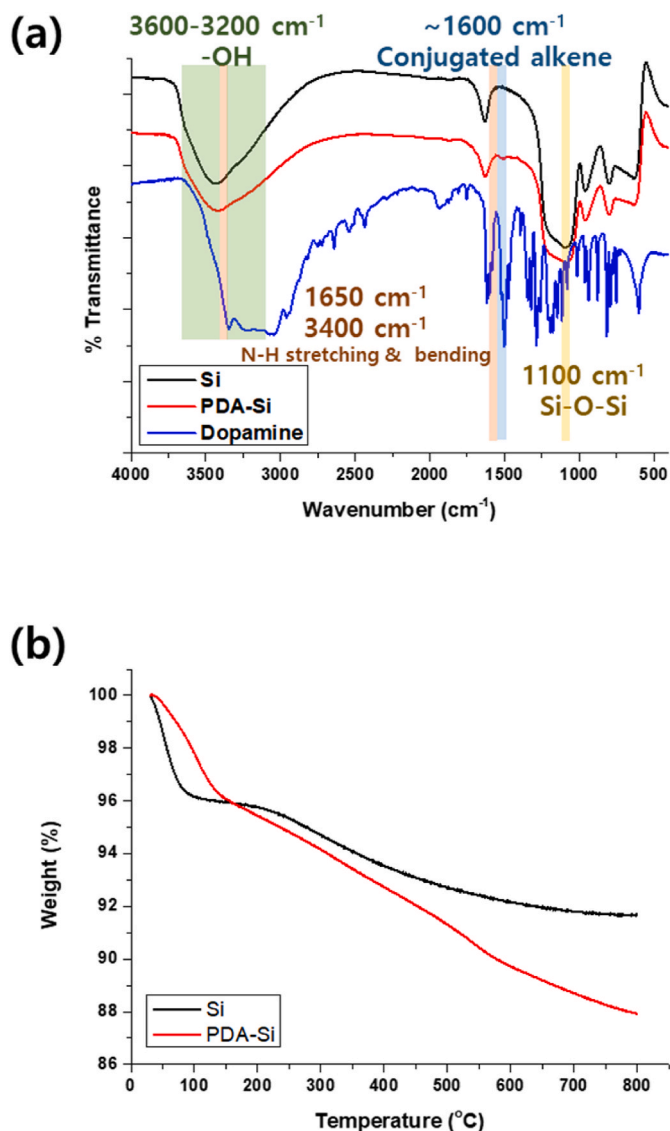


Fig. 2. (a) FT-IR spectra of the pure silica nanoparticle (Si, black), dopamine (Dopamine, blue), and polydopamine-coated silica nanoparticles (PDA-Si, red). (b) TGA curves of the pure silica nanoparticle and polydopamine-coated silica nanoparticles. (For interpretation of the references to colour in this figure legend, the reader is referred to the Web version of this article.)

5–15 nm, dopamine hydrochloride tris(hydroxymethyl)aminomethane, hydrochloric acid, and sodium (meta)periodate were purchased from Sigma-Aldrich (USA). Solvents, including tetrahydrofuran (THF), were purchased from Samchun Pure Chemical (South Korea). All chemicals were used as received without any further purification.

2.2. Synthesis of polydopamine-coated silica nanoparticle

Polydopamine-coated silica nanoparticles (PDA-Si) were obtained first by placing 1.0 g of silica nanoparticles and 80 mL of tris buffer base solution (pH 9.5) into a 250 mL round-flask and dispersed by tip-ultrasonication (SONOPLUS, Bandelin) for 20 min with a 20 s/10 s pulse cycle. Then, 200 mg of dopamine hydrochloride (1.30 mmol) and 34.9 mg of sodium (meta)periodate as an oxidant (0.163 mmol) were dissolved in a tris buffer solution before carefully being combined in the reaction flask. The flask was stirred at 600 rpm for 24 h at 25 °C. After stirring, the solution was filtered through a membrane filter, and the filtered particles were washed twice using ethanol and deionized (DI) water. The particles were dried overnight at 60 °C oven.

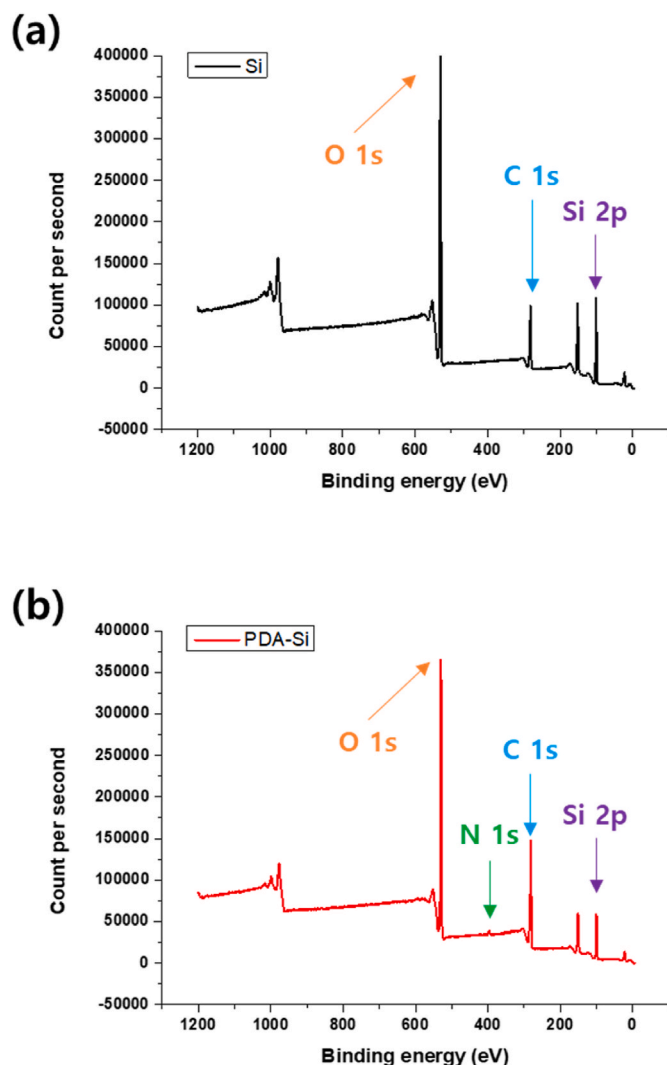


Fig. 3. XPS spectra of: (a) silica nanoparticle (Si), (b) polydopamine-coated silica nanoparticles (PDA-Si).

Table 2

XPS results for the atomic ratio of each nanoparticle.

Sample	C 1s (atomic %)	O 1s (atomic %)	N 1s (atomic %)	Si 2p (atomic %)
Si	3.95	84.39	–	11.66
PDA-Si	10.31	80.25	0.72	8.72

2.3. Fabrication of nanocomposite PSA films

PSA nanocomposite films were obtained through similar methods for the three sample types (neat; Si 3 wt%; and PDA-Si 3 wt%). To disperse 3 wt% of nanoparticles into acrylic PSA, 19.4 mg of PSA mixture and 0.6 mg of each nanoparticle (Si, PDA-Si) were placed into a vial. The nanoparticles were dispersed in the PSA mixture via tip-ultrasonicator (20 s/10 s pulse cycle) and vortex mixer (VM-10, DAIHAN Scientific) for 20 min. Next, the nanoparticle mixture was cast between release films, and the thickness was adjusted to 150 μm by a micro-film applicator. After that, the casted films were cured via a customized UV curing device (8.0 mW/cm²) for 5 min and stored in 60 °C oven for 24 h. The resultant thickness of film was 150 ± 30 μm.

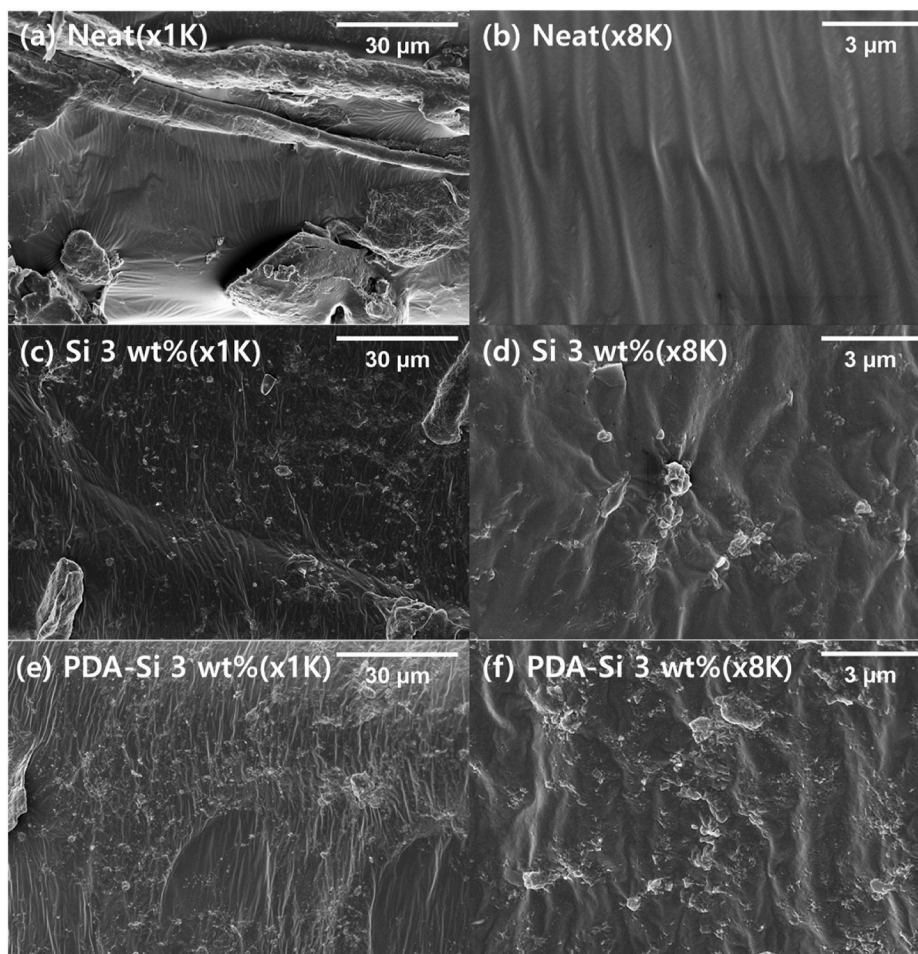


Fig. 4. FE-SEM images of the neat and nanocomposite PSA films. (a) Neat (x1000), (b) Neat (x8000), (c) Si 3 wt% (x1000), (d) Si 3 wt% (x8000), (e) PDA-Si 3 wt% (x1000), (f) PDA-Si 3 wt% (x8000).

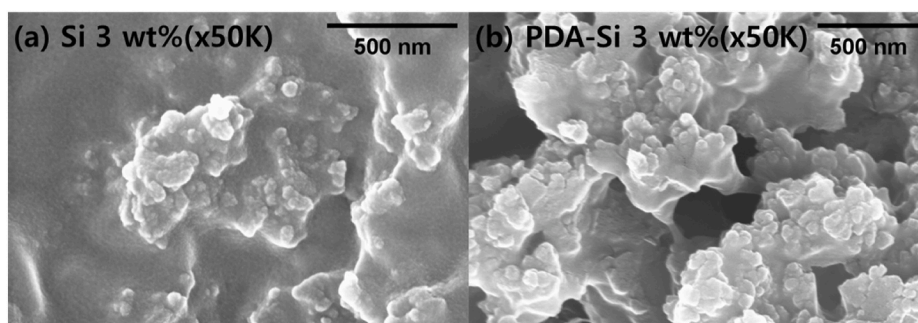


Fig. 5. High magnification FE-SEM images of nanocomposite PSA films. (a) Si 3 wt% (x50000), (b) PDA-Si 3 wt% (x50000).

2.4. Characterization of nanoparticles and nanocomposite PSA films

To observe the change of the nanoparticle surface through polydopamine coating, FT-IR (Nicolet, Thermo Scientific) in KBr mode, XPS (AXIS Supra+, Kratos Analytical), and TGA (Q50, TA instrument) were performed. FE-SEM (Supra25, Carl Zeiss AG) images were obtained to observe the dispersion of the nanoparticles in PSA films.

2.5. Gel content of the PSA films

To identify whether the crosslink density was changed due to the reinforcement of the silica nanoparticles by polydopamine coating, the

gel contents of each PSA film were measured via the following procedure. The initial weight (W_0) of the PSA films was measured before being placed into a vial and immersed in THF for 72 h to resolve the uncrosslinked contents of the PSA films. After immersion, THF was carefully removed by a PTFE membrane filter. Next, the residual film was dried at 60 °C in a vacuum oven for 24 h. Then, the final weight (W_f) was measured, and the gel contents were calculated as follows:

$$\text{Gel contents (\%)} = \frac{W_f}{W_0} \times 100 \quad (1)$$

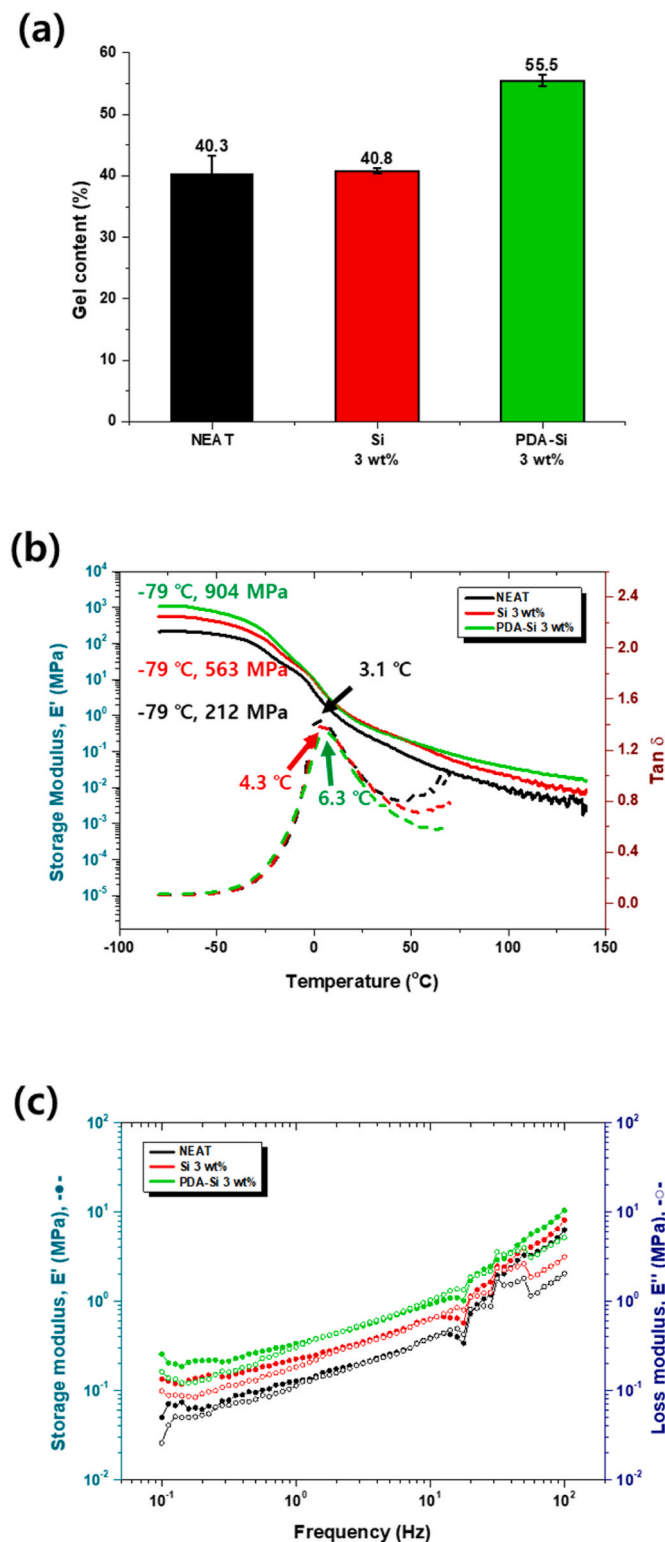


Fig. 6. (a) Gel content of the nanocomposite PSA films, (b) the temperature ramp curve of the nanocomposite PSA films (—: storage modulus, ---: $\tan \delta$), and (c) the frequency sweep curve of the nanocomposite PSA films by DMA (—●—: storage modulus, -○-: loss modulus).

2.6. Viscoelastic properties of the PSA films

DMA (TA instruments Q850) was used to characterize the viscoelastic properties of PSA films with a tension film clamp. Each PSA film ($L \times W \times T = 8 \text{ mm} \times 6 \text{ mm} \times 0.15 \text{ mm}$) was heated from -80°C to

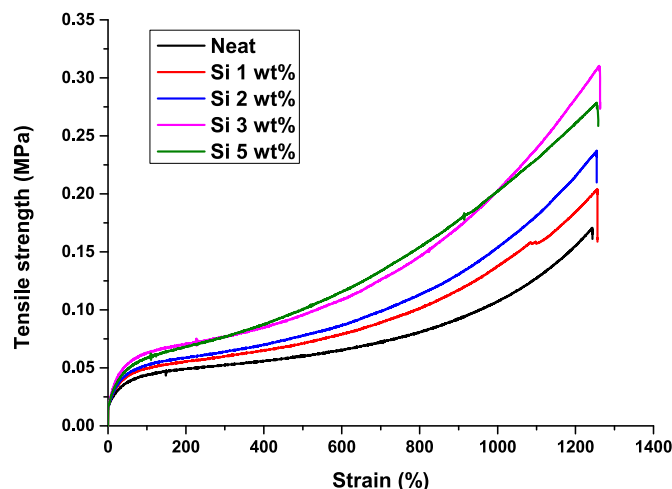


Fig. 7. Tensile stress-strain curves of the nanocomposite PSA films with 0 (neat), 1, 2, 3, 5 wt% of Si nanoparticles.

150°C at a ramp rate of $3^\circ\text{C}/\text{min}$ with $14.0 \mu\text{m}$ amplitude under constant frequency of 1 Hz. The maximum peak observed in the $\tan \delta$ curves was used to determine the glass transition temperature (T_g). The frequency sweep was performed from 0.1 to 100 Hz with 0.05% of strain at 30°C .

2.7. Mechanical properties of the PSA films

The tensile properties, including strength, strain, and modulus, were measured by a universal testing machine (UTM, DR-100, DRTECH) with reference to ASTM D638 [29]. The measurement was conducted at room temperature, and the crosshead speed was 20 mm/min. The maximum stress and initial slope until 5% of strain were used to represent tensile strength and tensile modulus, respectively. Five specimens were evaluated, and the average and standard deviation of the median three values, except maximum and minimum, were calculated.

2.8. Adhesive properties of the PSA films

Probe-tack testing was performed by ASTM D2979 [30] using a texture analyzer (TA.XT express, Stable Micro System Ltd.) equipped with an 11-mm-diameter stainless spherical probe. The test was conducted in 3 steps: approach, contact, and pull. The approach speed rate was 0.1 mm/s; the contact force was 35 N, where the contact time was around 4.5 s for all measurements, and the pull speed was 1.5 mm/s. During the pull stage, the maximum force value was recorded as probe-tack force.

The 180° peel strength test was conducted by ASTM D903 [31] using the same UTM as the tensile test. The film specimens were produced at the size of $25 \times 100 \text{ mm}^2$. One side of the fabricated films was covered by $25 \mu\text{m}$ of the PET film, while the other side was attached to the SUS 304 substrate. Then, a 2-kg rubber-roller was passed over the fabricated film back and forth twice. Because the peel strength is influenced by the dwell time in which the adhesive diffuses to the microstructure of the substrate, we compared the initial peel (30 min) and 24-h (24 h-) peel strength. Therefore, after 30 min and 24 h of stabilization, the specimens were measured at a crosshead speed of 200 mm/min. The average load value was used to indicate peel strength.

Lap shear strength was measured by ASTM C961 [32]. The PSA films were attached between 2 PET substrates that had a size of $25 \times 100 \text{ mm}^2$ with an overlap size of $12.5 \times 25 \text{ mm}^2$. Again, the rubber-roller was passed over back and forth twice. After 24 h of stabilization, the specimens were measured by another UTM (RB301, R&B Inc.) at a crosshead speed of 1.3 mm/min. Then, the maximum value was recorded to

Table 3

Average and standard deviation value of physical properties of the nanocomposite PSA films.

Sample	Tensile Strength (MPa)	Tensile Modulus (MPa)	Probe Tack (N)	Lap Shear Strength (MPa)	Initial Peel Strength (kgf/25 mm)	24 h-Peel Strength (kgf/25 mm)
Neat	0.168 ±0.007	0.081 ±0.011	18.47 ±0.35	0.390 ±0.029	2.236 ±0.078	2.257 ±0.021
Si 3 wt%	0.309 ±0.023	0.138 ±0.018	16.30 ±0.40	0.521 ±0.058	2.164 ±0.119	2.392 ±0.190
PDA-Si 3 wt%	0.474 ±0.020	0.176 ±0.012	11.13 ±0.79	0.613 ±0.010	2.111 ±0.115	2.429 ±0.139

represent the lap shear strength.

All measurements for both the mechanical and adhesive performances were conducted five times. The middle three values were used to obtain the average and standard deviation.

3. Results & discussion

3.1. Characterization of nanoparticles

The FT-IR spectra of the pure silica nanoparticles, dopamine, and polydopamine-coated nanoparticles (Si, DA, and PDA-Si) are shown in Fig. 2 (a). The characteristic peak of the Si–O–Si bonding at 1100 cm^{-1} (Yellow) was observed in each nanoparticle spectrum. Dopamine possesses an amine group, aromatic ring, and catechol group, which have distinguishable FT-IR peaks. Thus, the N–H stretching and bending at 3400 cm^{-1} and 1650 cm^{-1} (Orange), the conjugated alkene at 1600 cm^{-1} (Blue), and the O–H stretching at $3200\text{--}3600\text{ cm}^{-1}$ (Green) were well observed in the dopamine spectra. For PDA-Si, the peak of the hydroxyl group at $3200\text{--}3600\text{ cm}^{-1}$ was broadened by the presence of the catechol group in dopamine. Furthermore, the peaks of the amine and aromatic ring at $1600\text{--}1650\text{ cm}^{-1}$ were faintly visible.

Next, TGA curves were plotted, and they are shown in Fig. 2 (b). First, the pure silica nanoparticles showed about 4% of mass loss at $100\text{ }^{\circ}\text{C}$ because of the loss of atmospheric moisture. It gradually decreased to around 8% at $800\text{ }^{\circ}\text{C}$. When Si surface was coated with polydopamine, the trend of mass loss became considerably changed. In the PDA-Si curve, the steep decrease of mass at $100\text{ }^{\circ}\text{C}$ by atmospheric moisture loss was not observed due to the hydrophilic nature of polydopamine. The decomposition of polydopamine led to the continuous mass decrease until $800\text{ }^{\circ}\text{C}$ with a lower steepness, affording a higher percentage of mass loss than pure silica by approximately 12%.

The XPS results of each nanoparticle (Si, PDA-Si) are represented in Fig. 3 and summarized in Table 2. First, in the pure silica nanoparticle, the O 1s peak and Si 2p peak were dominant due to the Si–O–Si bond, accounting for 84.39% and 11.66%, respectively. The C 1s peak occupied a lower ratio of 3.95%. Moreover, the N 1s peak did not appear. When considering the polydopamine coating, the dominant O 1s and Si 2p peaks decreased to 80.25% and 8.72%, respectively, and the C 1s peak was increased to 10.31%. Most importantly, the 0.72% of the N 1s peak clearly appeared due to the nitrogen atoms in the polydopamine, suggesting successful incorporation of polydopamine on the Si surface.

3.2. Dispersion of nanoparticles in the nanocomposite PSA film

The surface morphology of each nanocomposite PSA film (neat, Si 3 wt%, and PDA-Si 3 wt%) was observed by FE-SEM at two kinds of magnification each as shown in Fig. 4. Firstly, we could see the inherent wrinkled surface morphology of neat PSA film in Fig. 4(a) and (b). By the adding 3 wt% of silica nanoparticles, we could observe the nanoparticles on the surface of PSA film as shown in Fig. 4(c) and (d). However, they were highly aggregated on the surface because the pure silica nanoparticles had strong particle-particle interactions each other. As represented in Fig. 4(e) and (f), polydopamine coated silica nanoparticles showed the better dispersion than the pure silica particles even though some portion of aggregations were still observed. These improvement

of dispersion can be explained by the enhanced interfacial interaction between nanoparticles and PSA films via polydopamine coating. As represented in Fig. 1(a), the polydopamine has a lot of hydroxyl groups in its molecular structure and the PSA films consist of acrylate monomers which can have strong molecular interaction with hydroxyl group. Furthermore, the abundant aromatic groups in polydopamine layer can improve the molecular interaction with terpene oil, the additive of PSA composition, as displayed in Table 1. Therefore, it could be expected that polydopamine coating improved the dispersion of nanoparticles as well as interfacial bonding with surrounded polymer chains in the nanocomposite films.

It was also demonstrated by observing the fracture surfaces with much higher magnification as shown in Fig. 5. We observed that the nanoparticles were highly aggregated and separated with PSA film in Fig. 5(a), which implied that pure silica nanoparticles and the surrounded acrylate polymers in PSA film had a poor interaction each other. On the other hand, the polydopamine coated silica nanoparticles seemed to be embedded in PSA film in Fig. 5(b). This means that polydopamine coating enhanced the interfacial interaction between nanoparticles and the surrounded polymer chains in PSA films and it improved the dispersion of nanoparticles as we demonstrated above.

3.3. Gel content of the nanocomposite PSA films

The results from the gel content examination of the PSA films are indicated in Fig. 6 (a). The neat PSA film had 40.3% gel content. The reinforcement of 3 wt% silica nanoparticles into the PSA film did not make a significant difference in the gel content (40.8%). However, with the polydopamine coating, the gel content substantially increased to 55.5%, implying that the pure silica nanoparticle had a weak physicochemical interaction with the molecular chain of the PSA film. In contrast, the polydopamine layer atop the silica surface produced better physicochemical interactions with the PSA chains, resulting in an enhancement of the gel content within the film. Based on the gel content analysis, the PDA-Si 3 wt% was thought to have the greatest mechanical properties among the three samples.

3.4. Viscoelastic properties of the PSA films

The temperature dependent viscoelastic properties of the PSA films are shown in Fig. 6 (b), which provide information about the modulus, T_g and cross-link density of each PSA film. The storage modulus (E') at $-79\text{ }^{\circ}\text{C}$ and T_g of neat PSA film was 212 MPa and $3.1\text{ }^{\circ}\text{C}$, respectively. After T_g , a rubbery plateau was observed indicating successful formation of crosslinked network. When 3 wt% silica nanoparticles were incorporated, both storage modulus at $-79\text{ }^{\circ}\text{C}$ and T_g were increased to 563 MPa (166% increment) and $4.3\text{ }^{\circ}\text{C}$, respectively. Also, the rubbery modulus (0.023 MPa) at $100\text{ }^{\circ}\text{C}$ became higher than that (0.008 MPa) of neat PSA film. After polydopamine coating, both storage modulus at $-79\text{ }^{\circ}\text{C}$ and T_g was further increased to 1070 MPa (405% increment) and $6.3\text{ }^{\circ}\text{C}$, respectively. Interestingly, the highest rubbery modulus (0.035 MPa at $100\text{ }^{\circ}\text{C}$) was observed for the PDA-Si 3 wt%. These results suggest that the polydopamine layer on the surface of the silica nanoparticles led to stronger interactions with the PSA polymer chains compared to that of pure silica surface, which resulted in enhanced cohesion of

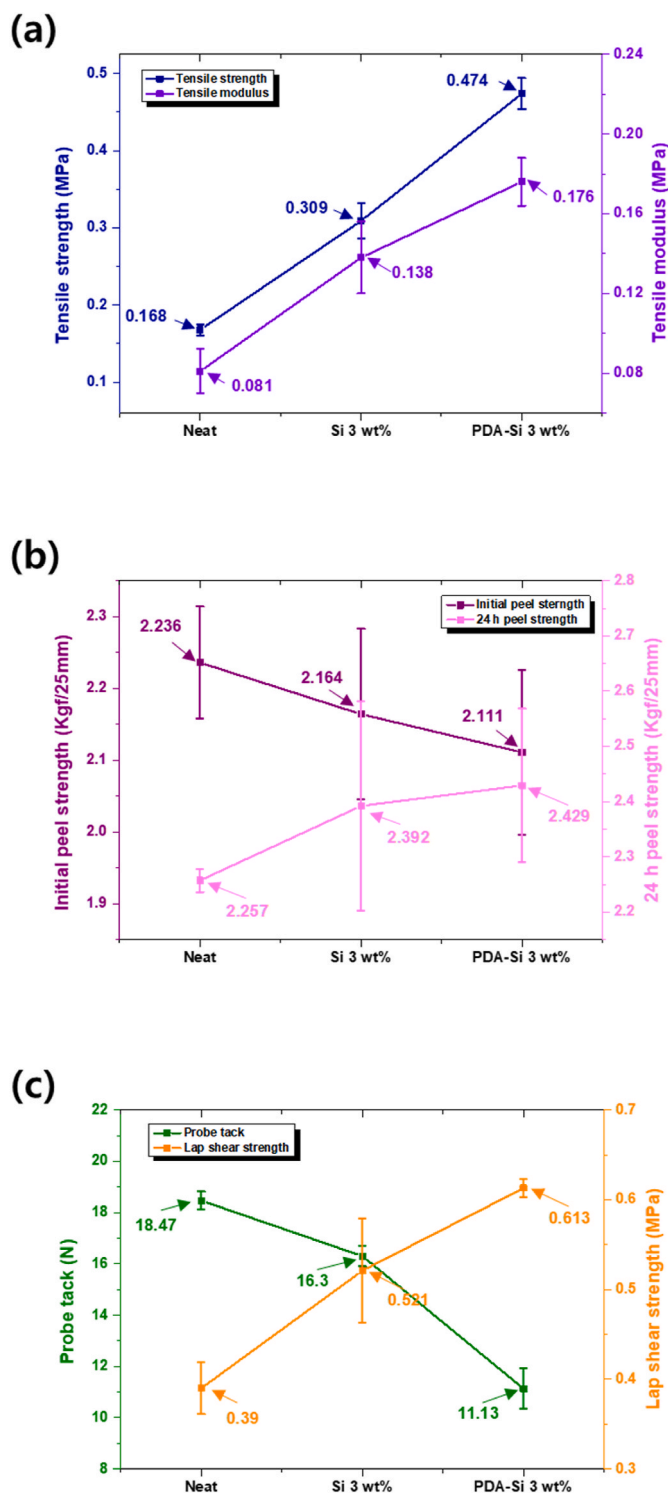


Fig. 8. Graphs for the average values of the (a) mechanical properties and (b) tack and lap shear strength (c) initial and 24 h- 180° peel strength of the nanocomposite PSA films.

nanocomposite PSA film and superior mechanical properties. Furthermore, the wettability of PSA film decreases with increasing the cohesion of the film in which the wettability is directly related with the experimental results of probe-tack test. Therefore, we could also predict that the PDA-Si 3 wt% would have the lowest tack force among the PSA films, which will be discussed in the later section on physical properties.

The frequency dependent viscoelastic properties of the PSA films are shown in Fig. 6 (c). The difference in viscoelastic property between the

Si 3 wt% and PDA-Si 3 wt% at 30 °C was obvious with the frequency sweep experiment, which was unclear in the temperature ramp curve at room temperature. The PDA-Si 3 wt% PSA film showed the highest values of storage and loss modulus, followed by the Si 3 wt% and the neat PSA film at all frequency range. Again, these results suggest that the PDA-Si 3 wt% displayed the greatest mechanical properties among three PSA films as discussed above in temperature ramp.

Especially in frequency sweep tests, we could correlate the specific frequency with the measurement condition of adhesive properties. Because the test condition of probe-tack and shear strength corresponds to low frequency region, we can predict the relative superiority of these two properties of the PSA films by comparing the storage modulus at low frequency. In the case of tack, the relative superiority can be easily predicted by wettability differences with the same principle in temperature ramp. Consequently, we could expect that PDA-Si 3 wt% would have the lowest tack force. In contrast, the shear strength can be simply predicted by comparing storage modulus at low frequency because shear modulus (G') is proportional to tensile modulus (E'). And we predicted that the PDA-Si 3 wt% would have the most superior shear strength among the PSA films.

3.5. Physical properties of the PSA films

In advance, we have evaluated the mechanical properties of the 1 wt %, 2 wt%, 3 wt%, 5 wt% of silica nanoparticles reinforced nanocomposite PSA films in order to find out the optimal weight fraction (wt %) of silica nanoparticles. As represented in Fig. 7, both tensile strength and modulus had improved until 3 wt%. However, when the 5 wt% of silica nanoparticles was reinforced, the mechanical properties were rather decreased than 3 wt% due to the aggregation of nanoparticles. Therefore, we concluded that the PSA film reinforced with 3 wt% of silica nanoparticles had the most superior improvement in effect in mechanical properties.

Test results for the mechanical properties are shown in Table 3 and Fig. 8(a). The neat PSA film had 0.168 MPa of tensile strength and 0.309 MPa of modulus, and it was very stretchable over 1200% of elongation. When the 3 wt% of silica nanoparticles were reinforced into the PSA film, the strength and modulus increased to 0.309 MPa and 0.138 MPa, showing 83.7% and 63.9% increase, respectively. This improvement was caused by the stress transfer from the PSA film to the nanoparticles when tensile force was applied. When the coated polydopamine was introduced on the nanoparticles, the strength and modulus dramatically increased to 0.474 MPa (181.9% increment) and 0.176 MPa (109.1% increment), respectively, as was previously predicted by the frequency sweep test of DMA. This remarkable improvement of tensile properties is because the stress was more effectively transferred by the polydopamine layer at the interfaces, and the strain was not affected by the reinforcement of nanoparticles.

The adhesive performance tests of each PSA film are also shown in Table 3 and Fig. 8(b). The neat PSA film had 18.47 N of probe tack. When reinforced with the 3 wt% silica nanoparticles, the tack slightly decreased to 16.30 N (11.7% decrement). The PDA-Si 3 wt% PSA film had the lowest tack force of 7.28 N (39.7% decrement). This decreasing trend is due to the numbers of attaching molecular chains of PSA affected by the interaction between the chains and nanoparticles, which is consistent with temperature ramp result in DMA indicating the increase of cohesion by polydopamine coating. And the tack showed the typical trade-off relationship with the mechanical properties.

The results of lap shear strength showed an opposite trend to the probe tack and peel strength, as represented in Table 3 and Fig. 8(b). The neat PSA film had 0.390 MPa of lap shear strength, and it increased to 0.521 MPa (36.1% increment) with the reinforcement of the 3 wt% of silica nanoparticles. The lap shear strength of the adhesive is a function of the ability to distribute or diminish the shear force and adhesive strength [33]. In the tests for the mechanical properties, we postulated that the silica nanoparticles acted as a stress transfer agent. Likewise, the

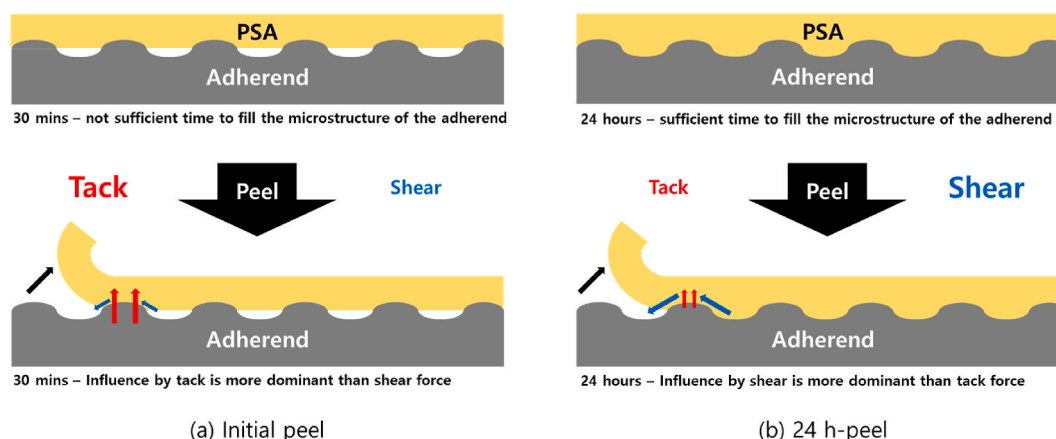


Fig. 9. Schematic diagram on influence of tack and shear force on peel strength during peel process. (a) Initial peel and (b) 24 h-peel.

reinforced nanoparticles could distribute the applied shear force; hence, the lap shear strength was increased. With polydopamine coating, the shear strength was further increased to 0.613 MPa (57.2% increment), and this improvement was also caused by the enhanced stress transfer by the polydopamine layer.

In the case of 180° peel strength indicated in Table 3 and Fig. 8(c), we measured the initial peel and 24 h-peel strengths. The initial peel strength showed a similar trend with the probe tack. The neat PSA film had an initial peel strength of 2.236 kgf/25 mm. With the addition of the 3 wt% silica nanoparticles, the initial peel slightly decreased to 2.164 kgf/25 mm (3.2% decrement). Furthermore, the 3 wt% polydopamine-coated nanoparticles had an even further decrease of 2.111 kgf/25 mm (5.9% decrement). In contrast, the 24 h-peel showed an opposite trend. The neat PSA film had a 24 h-peel strength of 2.257 kgf/25 mm. With the addition of the 3 wt% of silica nanoparticles, the 24-h peel slightly increased to 2.392 kgf/25 mm (6.0% increment). Moreover, with 3 wt% polydopamine-coated nanoparticles had a more increase of 2.429 kgf/25 mm (7.6% increment). These opposite results can be explained by an influence of time dependent tack and peel forces. The peel strength is combined result of the tack and shear forces, which forces exert differently according to the detail geometry of adhesive interfaces. As schematically shown in Fig. 9(a), the 30 min of dwell time for the initial peel test are not sufficient to fill the microstructure of the adherend by diffusion of PSA molecular chains. Then, the tack is more dominant than shear force during the peeling process because the contact surface is limited to only the top substrate area. Therefore, the results of the initial peel strength followed the trend of probe-tack in which the neat PSA film had the largest value of tack. On the other hand, the 24 h of dwell time are sufficient to fill the microstructure of the adherend as described in Fig. 9(b). Then the shear is more dominant than tack force because the whole area is in contact with the PSA film. As a result, the 24 h-peel strength had the same trend with shear strength in which the PSA film reinforced with 3 wt% polydopamine coated nanoparticles had the largest shear strength.

We confirmed that our prediction of mechanical and adhesive properties was consistent with final experimental results through the measurements of physical properties.

4. Conclusion

In this study, we investigated the effect of silica nanoparticles coated with polydopamine for the reinforcement of thin-film PSAs in overcoming the trade-off relationship between the mechanical and adhesive properties. We covered polydopamine on the surface of silica nanoparticles to fabricate the PSA nanocomposite film. Full characterizations were performed to confirm the functionalization of polydopamine on the nanoparticle surface. In doing so, it was confirmed that the

polydopamine layer enhanced dispersion and interface interaction between the nanoparticles and molecular chains of PSA. Besides, it was possible to predict the relative superiority concerning the physical properties of each PSA film by observing their viscoelastic behaviors, which were confirmed later by the test results of physical properties.

A considerable increase in the mechanical properties of the PSA film by approximately 180% was obtained, while the loss of initial peel strength was minimized by about 6% through the utilization of the polydopamine-coated silica nanoparticles. Further, we could overcome the trade-off relationship between mechanical and adhesive properties by enhancing 24 h-peel strengths. Therefore, the usefulness of polydopamine coating as a reinforcing method for thin-film PSA is verified. These results are promising for future research to lessen the effects of the trade-off relationship between mechanical and adhesive properties in PSA films.

CRediT authorship contribution statement

Seonghyun Kim: Methodology, Investigation, Data curation, Writing – original draft. **Seung Hui Lee:** Investigation, Data curation. **Subi Choi:** Investigation. **Suk-kyun Ahn:** Methodology, Investigation. **Gi-Deog Jang:** Resources, Methodology. **Jong S. Park:** Writing – review & editing, Supervision. **Dong Gi Seong:** Conceptualization, Writing – review & editing, Supervision, Funding acquisition.

Declaration of competing interest

The authors declare that they have no known competing financial interests or personal relationships that could have appeared to influence the work reported in this paper.

Acknowledgement

This work was supported by the Ministry of Trade, Industry and Energy and the Korea Evaluation Institute of Industrial Technology (10067433) and Basic Science Research Program through the National Research Foundation of Korea (NRF) funded by the Ministry of Education (NRF-2018R1D1A1B07045211).

References

- [1] J.-S. Kim, et al., Characterization and flexibility properties of UV LED cured acrylic pressure-sensitive adhesives for flexible displays, *J. Mater. Res. Technol.* 10 (2021) 1176–1183.
- [2] J.-H. Lee, et al., Adhesion performance and recovery of acrylic pressure-sensitive adhesives thermally crosslinked with styrene-isoprene-styrene elastomer blends for flexible display applications, *J. Ind. Eng. Chem.* 78 (2019) 461–467.
- [3] I. Benedek, M.M. Feldstein, *Technology of Pressure-Sensitive Adhesives and Products*, CRC press, 2008.

- [4] Z. Czech, R. Milker, Solvent-free radiation-curable polyacrylate pressure-sensitive adhesive systems 87 (2) (2003) 182–191.
- [5] K. Jin, et al., Improving the performance of pressure sensitive adhesives by tuning the crosslinking density and locations, *Polymer* 154 (2018) 164–171.
- [6] Q. Song, et al., Synergetic optimization of thermal conductivity and breakdown strength of boron nitride/poly (vinylidene fluoride) composite film with sandwich intercalated structure for heat management in flexible electronics, *Compos. Appl. Sci. Manuf.* 135 (2020), 105933.
- [7] Y. Wang, et al., Flexible printed circuit board based on graphene/polyimide composites with excellent thermal conductivity and sandwich structure, *Compos. Appl. Sci. Manuf.* 138 (2020), 106075.
- [8] W. Li, L. Bouzidi, S.S. Narine, Current research and development status and prospect of hot-melt adhesives: a review, *Ind. Eng. Chem. Res.* 47 (20) (2008) 7524–7532.
- [9] Z. Czech, M. Wojciechowski, The crosslinking reaction of acrylic PSA using chelate metal acetylacetonates, *Eur. Polym. J.* 42 (9) (2006) 2153–2160.
- [10] E.D.E.R. Hyde, et al., Colloidal silica particle synthesis and future industrial manufacturing pathways: a review, *Ind. Eng. Chem. Res.* 55 (33) (2016) 8891–8913.
- [11] T.-W. Kim, P.-W. Chung, V.S.Y. Lin, Facile synthesis of monodisperse spherical MCM-48 mesoporous silica nanoparticles with controlled particle size, *Chem. Mater.* 22 (17) (2010) 5093–5104.
- [12] J.J. Chruściel, E. Leśniak, Modification of epoxy resins with functional silanes, polysiloxanes, silsesquioxanes, silica and silicates, *Prog. Polym. Sci.* 41 (2015) 67–121.
- [13] Z. Tang, et al., Interface engineering toward promoting silanization by ionic liquid for high-performance rubber/silica composites, *Ind. Eng. Chem. Res.* 54 (43) (2015) 10747–10756.
- [14] J.H. Park, et al., Characteristics of transparent encapsulation materials for OLEDs prepared from mesoporous silica nanoparticle-polyurethane acrylate resin composites, *Compos. B Eng.* 175 (2019), 107188.
- [15] J. Abenojar, et al., Erosion-wear, mechanical and thermal properties of silica filled epoxy nanocomposites, *Compos. B Eng.* 120 (2017) 42–53.
- [16] S.K. Gupta, Failure load and stress intensity factor of single-lap steel joints bonded with nano-Al₂O₃ reinforced epoxy adhesive, *Funct. Comp. Struct.* 2 (2020), 035002.
- [17] H. Lee, et al., Mussel-Inspired Surface Chemistry for Multifunctional Coatings 318 (5849) (2007) 426–430.
- [18] P. Yang, et al., Recent developments in polydopamine fluorescent nanomaterials, *Mater. Horizons* 7 (3) (2020) 746–761.
- [19] J. Hu, et al., Polydopamine free radical scavengers, *Biomater. Sci.* 8 (18) (2020) 4940–4950.
- [20] M.B.M.Y. Ang, et al., Improved performance of thin-film nanocomposite nanofiltration membranes as induced by embedded polydopamine-coated silica nanoparticles, *Separ. Purif. Technol.* 224 (2019) 113–120.
- [21] W. Lee, J.U. Lee, J.-H. Byun, Catecholamine polymers as surface modifiers for enhancing interfacial strength of fiber-reinforced composites, *Compos. Sci. Technol.* 110 (2015) 53–61.
- [22] Y. Zou, et al., Boosting solar steam generation by photothermal enhanced polydopamine/wood composites, *Polymer* 217 (2021), 123464.
- [23] J.H. Lee, et al., Effects of monomer functionality on physical properties of 2-ethylhexyl acrylate based stretchable pressure sensitive adhesives, *Polym. Test.* 76 (2019) 305–311.
- [24] S. Sun, M. Li, A. Liu, A review on mechanical properties of pressure sensitive adhesives, *Int. J. Adhesion Adhes.* 41 (2013) 98–106.
- [25] P. Silva, et al., Effects of different environmental conditions on the mechanical characteristics of a structural epoxy, *Compos. B Eng.* 88 (2016) 55–63.
- [26] E. Karatas, et al., Synergetic effect of graphene nanoplatelet, carbon fiber and coupling agent addition on the tribological, mechanical and thermal properties of polyamide 6,6 composites, *Compos. B Eng.* 163 (2019) 730–739.
- [27] N.Z. Khalil, M.F. Johanne, M. Ishak, Influence of Al₂O₃ nanoreinforcement on the adhesion and thermomechanical properties for epoxy adhesive, *Compos. B Eng.* 172 (2019) 9–15.
- [28] Y. Hua, A.R.M. Kasavajhala, L. Gu, Elastic-plastic analysis and strength evaluation of adhesive joints in wind turbine blades, *Compos. B Eng.* 44 (1) (2013) 650–656.
- [29] Standard test method for tensile properties of plastics.
- [30] Standard test methods for pressure-sensitive tack of adhesives using an inverted probe machine.
- [31] Standard test method for peel or stripping strength of adhesive bonds, 2017.
- [32] Standard test method for lap shear strength of sealants.
- [33] L.F.M. da Silva, et al., Effect of adhesive type and thickness on the lap shear strength, *J. Adhes.* 82 (11) (2006) 1091–1115.